Geochimica et Cosmochimica Acta, Vol. 69, No. 15, pp. 3801–3811, 2005

0016-7037/05 $30.00 + .00

doi:10.1016/j.gca.2005.01.026

Strontium in coral aragonite: 3. Sr coordination and geochemistry in relation to skeletal architecture

NICOLA ALLISON,[1,*] ADRIAN A. FINCH,[1,2] MATTHEW NEWVILLE,[3] and STEPHEN R. SUTTON[3,4]

[1]School of Geography and Geosciences, University of St. Andrews, Irvine Building, St. Andrews, Fife KY16 9AL, UK
[2]Centre for Advanced Materials, University of St. Andrews, Irvine Building, St. Andrews, Fife KY16 9AL, UK
[3]Consortium for Advanced Radiation Sources, University of Chicago, Chicago, IL 60637, USA
[4]Department of Geophysical Sciences, University of Chicago, Chicago, IL 60637, USA

(*Received March* 22, 2004; *accepted in revised form January* 13, 2005)

Abstract—Use of the coral Sr palaeothermometer assumes that the Sr in coral skeletons is substituted randomly for Ca in the aragonite structure. The presence of Sr in additional phases e.g., strontianite, or the non random distribution of Sr across metal sites in aragonite, would complicate the Sr/Ca–sea surface temperature relationship. We have used Sr K-edge microEXAFS (extended X-ray absorption fine structure) to determine the structural state of Sr across selected microvolumes of four coral skeletons (*Porites lobata*, *Acropora palmata*, *Pavona clavus*, and *Montastrea annularis*). We used a 5 × 3 μm beam to analyse specific areas of the coral skeletal architecture, i.e., centres of calcification, fasciculi, and dissepiments. All EXAFS analyses refine, within error, to an ideally substituted Sr in aragonite, and we found no evidence of strontianite or partly ordered structural states. Anisotropy in the first shell responses results from the fact that the analysed microvolumes are not necessarily averaged for the responses of all crystal orientations in the aragonite. Although secondary ion mass spectrometry confirmed that Sr/Ca composition can vary substantially between skeletal components, we find no evidence for any contrast in Sr structural state. Sr heterogeneity may result from kinetic effects, reflecting complex disequilibrium processes during crystal precipitation, or biological effects, resulting from variations in the composition of the calcifying fluid which are biologically mediated.

1. INTRODUCTION

The aragonite skeletons of massive corals may record climatic information at the time of their deposition and have the potential to act as archives of past climates. The substitution of Sr for Ca in aragonite is temperature dependent, and the Sr/Ca ratios of fossil coral skeletons have been used as indicators of past sea surface temperatures (SSTs; e.g., Gagan et al., 1998). This approach assumes that the Sr in coral skeletons is substituted randomly for Ca in the aragonite structure. However, Greegor et al. (1997) suggested that Sr may also be present as strontianite ($SrCO_3$) domains. The presence of Sr in two phases (i.e., a mixture of strontianite and aragonite) or in partly ordered, intermediate states (i.e., single-phase materials in which Sr is not randomly distributed) would complicate the Sr/Ca-SST relationship. Understanding Sr structural state is therefore essential to maximise the potential of coral aragonite as a palaeoenvironmental archive.

To investigate the coordination of Sr in coral aragonite, we performed previously a series of experiments using Sr K-edge extended X-ray absorption fine structure (EXAFS) to determine Sr structural state in a variety of standard and coral materials (Finch et al., 2003a; Finch and Allison, 2003). We found no evidence of strontianite or intermediate states of Sr order in corals of different species, ages, and from a range of locations (Finch and Allison, 2003). However, these analyses were made on powdered bulk samples, and it remains possible that contrasts exist between different components of the coral skeleton. We estimated that the limit of detection of Sr in strontianite within aragonite is ~5% strontianite in these analyses (Finch et al., 2003). Some components of the coral skeleton (e.g., centres of calcification [COCs] and dissepiments) comprise <5% of the total aragonite volume, and alternative structural states associated with these skeletal components would not be resolved in bulk analyses.

In this paper we present a study of Sr structural state specifically related to coral skeletal architecture. We have used a microfocussed X-ray beam to carry out Sr K-edge microEXAFS in three discrete components of the skeleton: 1) in fasciculi, 2) in COCs, and 3) across a dissepiment. We aimed to determine if variations in Sr structural state occur between different skeletal features. We have also used ion microprobe analysis (or secondary ion mass spectrometry [SIMS]) to confirm variations in Sr/Ca concentration in each feature, and we are able to determine if Sr heterogeneity across the coral skeleton is accompanied by any variation in Sr structural state.

Fasciculi are formed from bundles of acicular crystals that are deposited over all surfaces of the precipitating skeleton during the day (Gladfelter, 1983). COCs are probably formed during the night (Cohen et al., 2001) by the accretion of small (approximately micron sized) equant randomly orientated crystals that are deposited at the axial spines of the corallite (Gladfelter, 1983). Dissepiments are accreted as layers ~2–3 mm from the coral surface and parallel to it. They are produced approximately monthly and seal off the bulk of the skeleton from the uppermost skeletal layer, which is still occupied by the coral tissue. Fasciculi make up the majority of the volume of the skeleton (>96%, Allison, 1996) and form the predominant component of bulk EXAFS analyses (Finch and Allison, 2003).

* Author to whom correspondence should be addressed (na9@st-and.ac.uk).

Table 1. Summary of the coral samples analyzed.

Coral species	Sample site	Reference number
Montastrea annularis	Puerto Rico	2T3[1,2]
Pavona clavus	San Cristobal, Galapagos	none[1,2,3]
Acropora palmata	Barbados	E6[1]
Porites lobata	Oahu, Hawaii	NA33[2,4]

References: 1 - Greegor et al. (1997); 2 - Finch et al. (2003); 3 - de Villiers et al. (1994); 4 - Finch and Allison (2003).

COCs are of particular interest in this study as they are relatively enriched in Sr compared to the surrounding fasciculi (Cohen et al., 2001; Allison and Finch, 2004). Contrasts in Sr structural state between COCs and fasciculi could explain this offset in Sr/Ca concentration. In addition, Cohen et al. (2001) suggested that COCs may provide a more reliable climatic proxy than fasciculi. If specific skeletal areas are to be targeted for palaeoenvironmental reconstructions, then it is of key importance that the Sr structural state within them is determined accurately.

2. MATERIALS AND METHODS

2.1. Sample Preparation

SIMS and microEXAFS analyses were performed on four coral specimens (Table 1) chosen to represent a selection of coral species, most of which are used in palaeoenvironmental reconstructions. MicroEXAFS was also performed on synthetic strontianite ($SrCO_3$). Thin sections of the corals were prepared by mounting strips (*Porites lobata*, *Pavona clavus*) or fragments (*Acropora palmata*, *Montastrea annularis*) of coral material on fused silica glass 2.54 cm (1″) round mounts (Heraeus Silica and Metals Ltd, UK) in epoxy resin and polishing to a thickness of 20–30 μm. Two thin sections were prepared from the *P. lobata* coral. The strips were cut parallel to the coral growth surface, one through a high-density skeletal band, deposited in the winter period (Schneider and Smith, 1982), and one through a low-density band, deposited during the summer. The material in each section would have been deposited within a narrow time frame. The *P. clavus* strip was cut parallel to the growth direction of the coral and perpendicular to the coral surface.

The sections were examined by optical microscopy, and potential areas for analysis were identified. Fasciculi and COCs can be readily identified in thin section, and the high spatial resolution of SIMS and microEXAFS potentially allows their analysis independently of the surrounding material. We carefully selected suitable areas for analysis, avoiding microborings, and selecting COCs that intersected the surface of the sample. The *P. clavus*, *M. annularis*, and *A. palmata* thin sections were analysed by SIMS after microEXAFS. Analyses were made adjacent (within 20 μm) to the microEXAFS analyses and sited on the same structures as analysed by microEXAFS. The *P. lobata* sections were analysed by SIMS before microEXAFS. Several SIMS transects were analysed across the *P. lobata* sections, but due to time constraints only one was subsequently analysed by microEXAFS. Because the COCs in this sample lie perpendicular to the plane of the section, they occupy a smaller surface area of the section. For this reason, microEXAFS analyses were made directly over the SIMS analysis pits. Au coats, required for SIMS, were removed from the sections before EXAFS analysis.

The strontianite was sprinkled as a powder onto sticky tape, and samples were formed from the repeated superposition of tape layers to seek an even sample thickness. A subsample of one coral (*M. annularis*) was also ground to a powder and mounted in this way.

2.2. MicroEXAFS Data Collection

All samples were analysed at Sector 13, GeoSoilEnvironCARS at the Advanced Photon Source, Argonne, Illinois, USA. The Advanced Photon Source synchrotron has a 7-GeV machine energy, and had a typical current of ~90 mA during measurements. Station 13ID uses a 72-period undulator and a Si(111) monochromator. The beam was focussed to a circular spot of ~15 μm^2 using Kirkpatrick-Baez mirrors described by Eng et al. (1998). The X-rays generated by the synchrotron are horizontally polarized. Each sample was mounted on a motorised stage at 45° to the incident X-ray beam and to the detector; the detector is at 90° to incident beam and within the horizontal plane of the synchrotron (see Sutton et al., 2002, for further details of the experimental line used). Because the surface of the sample lies at 45° to the beam, the beam excites an elliptical spot on the surface ~3 μm high × 5 μm wide. We estimate that the excited X-ray microvolumes (the area of the spot times the depth of the sample when mounted at 45° to the beam) were ~420–630 μm^3. The strontianite standard was measured in transmission mode, whereas all other materials were measured as Sr Kα fluorescence with a 16-channel Ge solid-state detector. Two or three scans were amalgamated to provide the final spectra. The monochromatic X-ray beam was scanned across the Sr K absorption edge between 16.08 and 16.40 keV at 1.5-eV intervals, with a 2 s residence time per point. Note that count times were not extended with k, and each sample took typically 2 h of beamtime to run. Significant spikes in the intensity of the primary X-ray beam (I_0) were systematically observed at ~16.35 and 16.55 keV due to other silicon lattice planes coming into the Bragg condition, leading to glitches in the microEXAFS data that were incompletely removed by normalization. All data were deglitched in these energy regions before analysis by the deletion of affected data points.

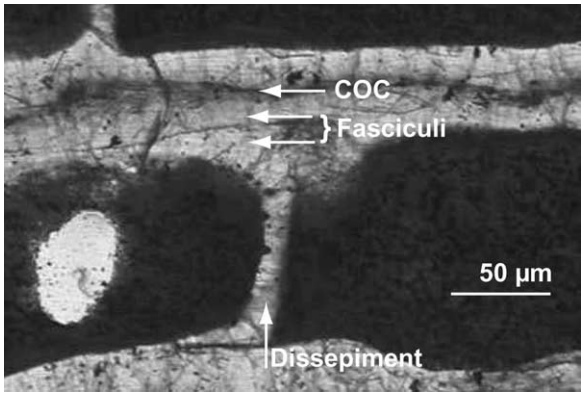

Fig. 1. Transmitted light photomicrograph of the *Pavona clavus* thin section with locations of microEXAFS analyses indicated by white arrows. Arrow direction indicates the direction of the X-ray beam. This section was gold-coated after analysis, and the epoxy resin, between skeletal elements, appears black.

MicroEXAFS of COCs and adjacent fasciculi were made on the *M. annularis*, *P. lobata*, and *P. clavus* thin sections. The beam was positioned so that one set of analyses was made along a COC in each slide and two sets of analyses were made along adjacent fasciculi (Fig. 1). The *P. clavus* sample was then rotated by 90°, and an additional analysis was made across a single dissepiment (Fig. 1). Powdered samples were analysed by placing the centre of the tape layers in the path of beam.

Traverses of analyses, crossing fasciculi and COCs, were also performed across the *P. lobata* and *A. palmata* thin sections (Figs. 2 and 3). We performed these traverses at approximate 10-μm intervals to explore whether gradual changes in refinement parameters could be observed as the traverse encountered the COC. This might give evidence for contrasting structural states between these and the fasciculi. The interaction between the X-ray beam and the sample caused the formation of colour centres in the aragonite, so that the microvolume analysed could be later identified by optical microscopy.

To estimate the maximum contributions of background counts from the epoxy resin and the silica slide, analyses were completed on spots where coral filled the depth of the section, where epoxy resin filled the depth of the section, and on an area of the silica slide containing no coral and no epoxy resin. The percentage of X-ray transmission through

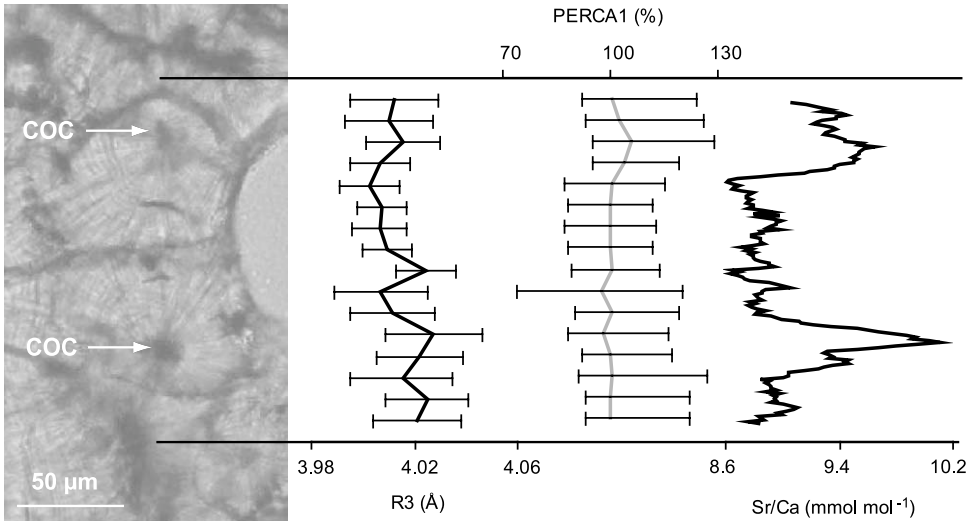

Fig. 2. The microEXAFS and SIMS traverse across the *P. lobata* section, cut from a low-density annual band. The transmitted light micrograph on the left indicates the position of the traverse (bounded by the solid black lines) with centres of calcification (COC) marked. Variations in R3 and PERCA1 across the microEXAFS traverse are shown with estimated errors.

the sample is dependent on the sample composition, density, its effective thickness (a product of thickness and porosity), the incident beam energy, and the emitted fluorescence energy. The primary beam encounters the sample at 45°, and the analytical depth observed in different sections varied between 28 and 42 μm. We estimate that the percentage of secondary Sr Kα X-ray transmission through the sample from these depths in aragonite (ρ = 2.94 g cm^{-3}) is 57% and 43% respectively (Criss, 1977). Sr count rates from the silica slide were ~5% of count rates observed on the coral. The contribution of counts from the silica slide to an analysis is less than this (~3–4%) as the coral overlying the silica slide absorbs some of the counts generated from the slide. Sr count rates from areas of the section filled with epoxy resin were ~2% of count rates observed on areas of the section filled with coral. We selected areas for analysis where coral appeared to fill the depth of the section, but we estimate that a layer of epoxy resin of 5 μm thickness behind coral of 25 μm thickness would contribute <0.5% to the Sr counts from the coral. Therefore, the EXAFS we observed can be attributed almost entirely to the coral aragonite in the illuminated volume.

2.3. MicroEXAFS Data Analysis

Data analysis was carried out using programs provided by Daresbury Laboratories, Warrington, UK. The intensity of the primary X-ray beam (I_0) was generally stable but even so the fluorescence data were normalized to I_0. Backgrounds were removed from the data using SPLINE (Paul Ellis, University of Sydney, 1990), and phase-shifted Fourier transforms of the data to provide the radial distribution functions were carried out using EXCURV98 (Daresbury Laboratories, UK). Interatomic distances and Debye-Waller factors were refined to minimise the squares of residuals between the unfiltered data and the model spectrum using single scattering on EXCURV98. Refinements

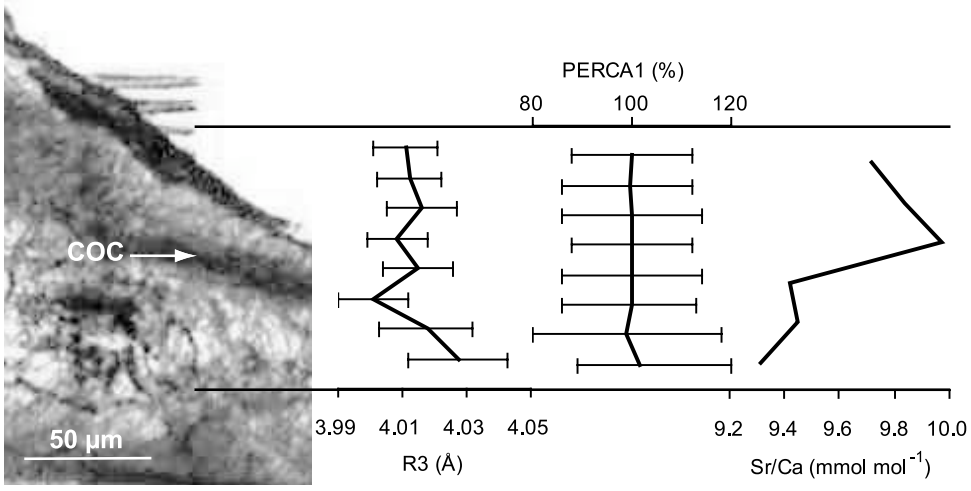

Fig. 3. The microEXAFS and SIMS traverse across the *A. palmata* section. The transmitted light micrograph on the left indicates the position of the traverse (bounded by the solid black lines) with COC marked. The horizontal burn marks at the top of the image indicate the position of the EXAFS X-ray beam as the traverse crossed the epoxy resin. Variations in R3 and PERCA1 across the microEXAFS traverse are shown with estimated errors.

were carried out within a k-range of 2 to 10 and an R range of 1.6 to 4.5 Å. Bulk EXAFS data were refined previously over a k-range of 2 to 11 (Finch et al., 2003a), but an analysis of the relationship between fit index and the uppermost limit of k (KMAX) in the microEXAFS data indicated that a reduced k-range provided the best balance between expanding the k-range (so maximising the determinacy) and reducing noise (more problematic at higher k). Refinements were carried out with a k^3 weighting. Under these conditions, the numbers of independent parameters supported by the data ($N = 2\Delta k \Delta R/\pi + 1$) are ~15.7, significantly greater than the numbers of variables in the fitting procedure (P = 8), giving a determinacy (N/P) of ~2. The fit index (R) is defined as:

$$R = \sum_i \left[\frac{1}{\sigma_i} \left\{ \left| \chi(\text{exp})_i - \chi(\text{theory})_i \right| \right\} \right] \times 100\%$$

where

$$\frac{1}{\sigma_i} = \frac{k_i^3}{\sum_i \left[k_i\right]^3 \times \left| \chi(\text{exp})_i \right|}$$

Errors relate to the average displacements in each value required to cause a 2.5% increase in the optimum fit index. The summaries of all the refinements are presented as an electronic annex to the present article showing $k^3\chi(k)$ and FT $k^3\chi(k)$ for data and corresponding fits.

2.4. Developing Refinement Procedures and Protocols

Coral skeletons are highly organised structures, and on micron scales the crystals within them are not randomly orientated. During the analysis of powders the polarization dependence of the EXAFS is averaged over all sample orientations, but in analysis of thin sections this does not occur. In previous papers, we optimised refinement procedures for powdered samples, but in the present study we use alternative procedures, more appropriate for microEXAFS data. To confirm that the change in refinement protocol does not affect our data interpretation, we refine the data from the powdered strontianite and *M. annularis* samples using both procedures and demonstrate that there is no significant difference in the final refinement parameters.

During refinement, modelling compares the observed data with a theoretical spectrum generated by a series of crystallographic parameters. Minimizing the difference between the two using a least squares procedure refines the model against the data. Finch et al. (2003a) established a structural model for aragonite against which EXAFS refinement could be made. Aragonite is a low symmetry (orthorhombic) mineral with several nonequivalent crystallographic sites, but refinement of aragonite EXAFS can be achieved by averaging nonequivalent sites and assuming rhombic symmetry. This reduces the number of shells in the refinement to three, i.e., a first shell of oxygens, a second shell of carbons, and a third shell of calcium and/or strontium atoms. The variables refined in the Finch et al. (2003a) model are the Sr K-edge energy (E_f), the interatomic distances between the central Sr and the nearest neighbour atoms (R_1, R_2, and R_3) and the Ca:Sr population of the atoms in the third shell (PERCA1, scaled to be 100% for all Ca and 0% for all Sr). In addition, the model requires isotropic Debye-Waller parameters (σ^2_1, σ^2_2, and σ^2_3) and the number of atoms for each shell (the coordination number, N_1, N_2, and N_3). The Debye-Waller factors include thermal disorder (i.e., thermal vibration around a central position) and static disorder (i.e., uncertainties caused by averaging several nonequivalent atomic positions) for each site. To refine N and σ^2 simultaneously would increase the number of variables in each refinement (P) to 11, significantly reducing the determinacy of the refinement (N/P = 1.43). In addition, the Debye-Waller parameters (σ^2) are correlated to coordination (N) so that meaningful simultaneous refinement is difficult. To maintain the determinacy of the refinements, we fix one of these two parameter sets and refine the other. For bulk analyses (e.g., Finch et al., 2003a), the coordination is fixed from the stoichiometry of aragonite (N_1 = 9, N_2 = 6, and N_3 = 6) and the isotropic Debye-Waller parameters (σ^2_{1-3}) are refined. However, in refining microEXAFS data, it is incorrect to assume that N_{1-3} are fixed by aragonite stoichiometry, as crystal orientations are unlikely to be random. Some orientations may be preferentially represented in the data at the expense of others, leading to values of N different from the average stoichiometry. It is difficult to estimate the possible variations in inferred N that would result from orientation dependence of a single crystal in the polarised beam. Some planes around the central Sr in aragonite (e.g., (001)) contain no first or second shell atoms, whereas others (e.g., (111)) contain a greater than average number. Furthermore, aragonites are repeatedly twinned on {110} form faces, making estimates of the variation in N difficult. In the present study, therefore, we have fixed σ^2_{1-3} and refined N_{1-3}, with values of σ^2_{1-3} taken from bulk analysis of an aragonite standard (Finch et al., 2003a). A slight weakness in this approach is that values of σ^2 in Finch et al. (2003a) are assumed to be isotropic.

To confirm that the change in refinement protocol does not affect our data interpretation, we have refined the powdered samples using both procedures and compared the results (Table 2, Fig. 4). It is exceptionally difficult to make powdered samples that are truly homogeneous on micron scales. The refinement parameters mostly conform to results expected of bulk, but a few (e.g., N_1 and σ^2_1 in strontianite, Table 2) lie outside the expected range in stoichiometry or the isotropic Debye-Waller factors of the bulk (Finch et al., 2003a). This suggests that, despite our best efforts, the powdered samples are not entirely homogeneous and that clumps or pinholes exist in the sample at micron scales. However, the fit indices by each protocol are similar and the values of the common parameters (E_f, R_{1-3}, PERCA1) overlap within error. We conclude that either protocol provides satisfactory modelling of the microEXAFS of powders. We have then used both protocols to refine data from a *P. clavus* thin section in which we analysed the same microvolume, but rotated the section by 0, 45, and 90° between each analysis (Table 3). In those data, sample anisotropy is marked, particularly in parameters associated with the first shell. Refinements in which N are varied and σ^2 are fixed generally gave better fit indices, and values of PERCA1 closer to 100%. We therefore fix σ and refine N in the refinements presented in the present study.

The microEXAFS data have higher R-factors than the corresponding bulk analyses previously published (Finch et al., 2003a). For example, the refinements of strontianite and *M. annularis* powders by

Table 2. Refinements of microEXAFS of powdered strontianite and *Montastrea annularis*, using fixed N and fixed σ^2 refinement protocols.

Strontianite powder refinements			
	σ^2 fixed		N fixed
E_f	−6.54 ± 0.32	E_f	−6.51 ± 0.32
N_1	8.48 ± 0.44	σ^2_1(Å^2)	0.031 ± 0.002
N_2	6.77 ± 0.91	σ^2_2(Å^2)	0.022 ± 0.005
N_3	4.32 ± 1.50	σ^2_3(Å^2)	0.040 ± 0.006
R_1(Å)	2.646 ± 0.005	R_1(Å)	2.651 ± 0.006
R_2(Å)	3.046 ± 0.015	R_2(Å)	3.053 ± 0.014
R_3(Å)	4.163 ± 0.025	R_3(Å)	4.163 ± 0.024
R (Fit)	33.0%	R (Fit)	32.8%
M. annularis powder refinements			
	σ^2 fixed		N fixed
E_f	−9.23 ± 0.32	E_f	−9.12 ± 0.34
N_1	9.27 ± 0.48	σ^2_1(Å^2)	0.024 ± 0.002
N_2	7.71 ± 1.16	σ^2_2(Å^2)	0.043 ± 0.013
N_3	6.02 ± 1.17	σ^2_3(Å^2)	0.024 ± 0.005
R_1(Å)	2.580 ± 0.006	R_1(Å)	2.580 ± 0.006
R_2(Å)	2.955 ± 0.022	R_2(Å)	2.943 ± 0.030
R_3(Å)	4.017 ± 0.016	R_3(Å)	4.014 ± 0.016
PERCA1	96 ± 14%	PERCA1	89 ± 10%
R (Fit)	32.0%	R (Fit)	30.4%

For fixed N refinements, N values were N_1 = 9, N_2 = 6, N_3 = 6, and for fixed σ^2 protocols, the values used were σ^2_1 = 0.022 Å^2, σ^2_2 = 0.038 Å^2, and σ^2_3 = 0.028 Å^2 (Finch et al., 2003a).

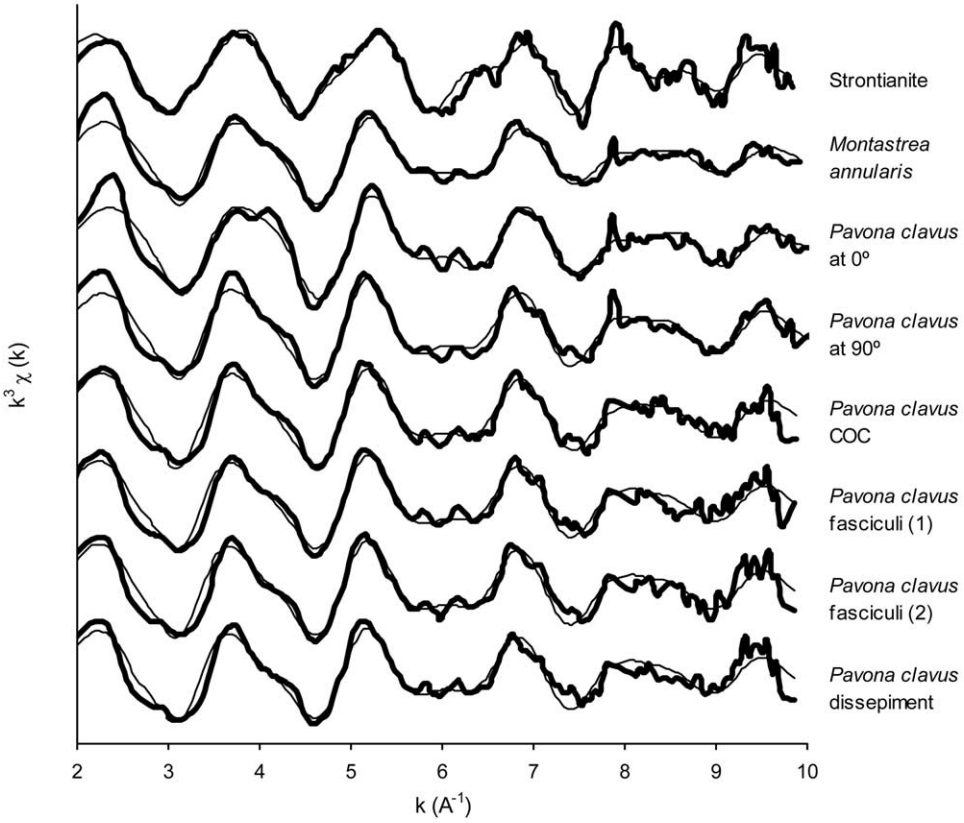

Fig. 4. Isolated EXAFS oscillations for a selection of the data. The bold lines are the raw data and the fine lines are model EXAFS based on the fits generated by refinement parameters in Tables 2, 3, and 5 using the fixed σ^2 protocol. Strontianite and *Montastrea annularis* refinement parameters are given in Table 2, the *Pavona clavus* at 0° and 90° orientations are from Table 3, and the data for *Pavona clavus* centres of calcification (COCs), fasciculi, and dissepiments correspond to the areas identified in Figure 1 and refinement parameters shown in Table 5.

microEXAFS provide R-factors ~30–33% (Table 2), whereas bulk data had R-factors of ~23–24%. This is because count times were not extended with k during microEXAFS, in contrast to the procedure used with the collection of the earlier bulk data. Although the microEXAFS data have a greater amount of random noise, refinement of both datasets provides indistinguishable final parameters.

The Sr coordination state of the samples, the focus of the present study, is distinguished by refinement values associated with the third shell: R_3, N_3, and PERCA1 (Finch et al., 2003a). R_3 represents the interatomic distance between the central Sr and its nearest metal, which in the aragonite coordination is ~4.018 ± 0.010 Å, and in strontianite is 4.167 ± 0.010 Å. N_3 is the effective coordination around the central Sr, which is 6 in the stoichiometric material but may vary significantly in the microEXAFS refinements. The parameter PERCA1 is scaled to vary such that 0 Sr atoms in the third shell (i.e., aragonite) corresponds to PERCA1 = 100%, and 6 Sr (i.e., strontianite) is represented by PERCA1 = 0%. Two-phase states or partly ordered structural states are readily observable in EXAFS as deviations of R_3 and PERCA1 from the values for the appropriate standard (Finch et al., 2003a). The errors in refinable values associated with the third (metal) shell in these powdered samples are typically ~1.3 (N_3), 0.022 Å (R_3), and 12% (PERCA1). If spectra of mixed coordination are refined as single-phase materials, the resultant values of R_3 increase from ~4.012 Å in single-phase aragonite towards 4.163 Å in strontianite (Table 2). Note that values greater than 4.163 Å can be produced if the model uses Ca phase shifts when Sr phase shifts are appropriate. PERCA1 values would fall from 100% (aragonite) towards 0% (strontianite). Importantly, the average errors in N_3, R_3 and PERCA1 would substantially increase (e.g., double) as the refinements attempted to resolve strontianite-type and aragonite-type third shells into a single averaged entity. Where dual-phase mixtures are suspected, the data can be refined as mixtures of aragonite and strontianite, using parameters for these materials taken from standards (Finch et al., 2003a) and refining the edge energy (E_f) and the relative proportions of the two phases. The interatomic distances determined by EXAFS refinements are based on ab initio calculations derived from phase shifts and can deviate from distances deduced by diffraction methods. The strontianite interatomic distance has been determined independently by neutron diffraction (Jarosch and Heger, 1988) as 4.162 Å, indistinguishable from the observed value from EXAFS (4.163 ± 0.025 Å, Table 2).

2.5. SIMS

Sr/Ca ratios were determined using a Cameca ims-4f ion microprobe (University of Edinburgh, UK). Sections were gold-coated and analysed with a $^{16}O^-$ ion beam, accelerated at 14.5 kV. Sr/Ca ratios in the *P. lobata* specimen were determined in line scan mode along transects which crossed fasciculi and COCs. The remaining sections were analysed in spot mode, with spots focussed on individual structures. The analytical conditions are summarised in Table 4. A field aperture was inserted between the sample and the mass spectrometer, to restrict the area from which secondary ions were collected to ~10 μm in spot mode and to ~5–10 μm in line scan mode. A contrast aperture restricted the angular spread of ions so that ion focussing aberrations did not degrade the effective spatial resolution. Secondary ions of Ca^+ and Sr^+ were collected at masses 44 (counting time 2 s) and 88 (counting time 2 s) respectively in each analytical cycle. Typical count rates at masses 44 and 88 were 6,000,000 and 1,900,000 cps respectively in spot mode and 160,000 and 50,000 cps in line scan mode. We estimate the possible contribution of $^{44}Ca^{44}Ca$ species to the counts at

Table 3. Refinements of a microvolume of *Pavona clavus* thin section as a function of the orientation of the slide with respect to the plane of polarization in the X-rays.

	Refinements with fixed N and refined σ^2		
	0°	45°	90°
E_f	−9.20 ± 0.36	−8.89 ± 0.38	−9.65 ± 0.39
σ^2_1(Å^2)	0.022 ± 0.002	0.019 ± 0.002	0.018 ± 0.002
σ^2_2(Å^2)	0.064 ± 0.021	0.040 ± 0.014	0.038 ± 0.013
σ^2_3(Å^2)	0.026 ± 0.004	0.022 ± 0.005	0.026 ± 0.005
R_1(Å)	2.565 ± 0.006	2.582 ± 0.006	2.596 ± 0.006
R_2(Å)	2.902 ± 0.047	2.894 ± 0.034	2.945 ± 0.033
R_3(Å)	4.012 ± 0.013	4.013 ± 0.016	4.022 ± 0.015
PERCA1	123 ± 20%	100 ± 18%	118 ± 22%
R (Fit)	30.3%	35.4%	32.6%
	Refinements with fixed σ^2 and refined N		
	0°	45°	90°
E_f	−10.25 ± 0.31	−9.36 ± 0.35	−9.87 ± 0.33
N_1	10.44 ± 0.53	11.47 ± 0.63	11.23 ± 0.55
N_2	7.82 ± 1.36	8.13 ± 1.53	9.26 ± 1.38
N_3	7.78 ± 1.22	8.79 ± 1.67	7.82 ± 1.27
R_1(Å)	2.579 ± 0.006	2.597 ± 0.006	2.603 ± 0.005
R_2(Å)	2.985 ± 0.026	2.986 ± 0.025	2.995 ± 0.020
R_3(Å)	4.022 ± 0.013	4.021 ± 0.015	4.025 ± 0.014
PERCA1	100 ± 16%	103 ± 15%	98 ± 12%
R (Fit)	30.9%	33.4%	30.4%

The data are refined using both fixed N and fixed σ^2 refinement protocols. For fixed N refinements, N values were $N_1 = 9$, $N_2 = 6$, $N_3 = 6$, and for fixed σ^2 protocols, the values used were $\sigma^2_1 = 0.022$ Å^2, $\sigma^2_2 = 0.038$ Å^2, and $\sigma^2_3 = 0.028$ Å^2 (Finch et al., 2003a).

mass 88 as <0.2% of ^{88}Sr counts, and we have made no correction for this in estimating Sr concentrations.

In spot mode we used a presputter or "burn-in" time of 3 min to remove surface contamination, and then data were collected over 15 analytical cycles. The total time per analysis (including other isotopes not reported here) was 10 min, and during this time the primary beam sputtered the sample to a depth of <5 μm. The relative ion yield of Sr to Ca was estimated after multiple analyses on an OKA carbonatite standard (Sr/Ca = 13.1 mmol mol^{-1}). Internal reproducibility (the Sr/Ca precision at a single point) was calculated from 2 standard deviation(s) of the 15 cycles in each analysis divided by $\sqrt{15}$ and was typically 0.5% on the coral sample. External reproducibility (the precision of 10 analyses on the standard) was typically 0.3%.

To remove surface contamination in line scan mode, we moved a 20-nA beam along the selected transect at 1-μm intervals with a burn time of 30 s per interval. For data collection, we refocused the beam using the conditions in Table 4 and collected data at 1-μm intervals, running one analytical cycle per interval. Sr/Ca ratios were standardised by performing 2 or 3 spot analyses next to each line. We discarded any data that were collected within 10 μm of the edge between the coral and the surrounding epoxy resin.

Table 4. Analytical conditions for SIMS line and spot analyses.

	Line analyses	Spot analyses
Primary beam current (nA)	0.3	6
Energy offset (eV)	0	0
Imaged field (μm)	25	25
Field aperture	3	2
Contrast aperture	3	1

SIMS = secondary ion mass spectrometry.

3. RESULTS AND DISCUSSION

3.1. Sr Coordination in Relation to Skeletal Architecture

The EXAFS refinements and SIMS analyses on the fasciculi and COCs of *M. annularis*, *P. clavus*, and *P. lobata*, and a dissepiment of *P. clavus* are summarised in Table 5. The points analyzed in *P. clavus* correspond to Figure 1. The isolated EXAFS of these data and their refinements are shown in Figure 4. SIMS indicated that all the COCs contained more Sr/Ca and that the dissepiment had a similar Sr/Ca composition to the surrounding fasciculi (Table 5). The values of R_3 and PERCA1 refine to values within error of a single-phase aragonite (R_3 = 4.012 Å, PERCA1 = 100%). The fit indices are all good, and average errors in N_3, R_3, and PERCA1 are typically ~1.4, 0.016 Å, and 20% respectively, similar to values observed in powdered materials (Table 2). We observed variation in N values between points, which accommodate differences in the anisotropies of the microvolumes analyzed. Some points (e.g., the *M. annularis* COC) have optimum PERCA1 >100%, the value that indicates that all neighbouring metal sites are occupied by Ca atoms. Values >100% can be generated during refinement but have no physical meaning over and above total occupancy by Ca as "stuffed" crystal aragonites, with excess interstitial metal cations, are not known. Under these circumstances, we might fix PERCA1 to 100%, the maximum value with a physical meaning, and refine other variables. The drawback of such an approach is that the determinacy of refinements with PERCA1 > 100% becomes different to those where PERCA1 ≤ 100%, and therefore errors cease to be directly comparable. In addition, the reader under such circumstances is unclear whether the refinement minimized to a value close to 100% (e.g., 102%), or whether that value would have converged to unrealistic values (e.g., 200%), which might indicate failings in the model being applied. In the present study, we present all refinements with the same number of floating variables and accept that this results in some PERCA1 values >100%.

The refinements of the microEXAFS, with corresponding SIMS analyses, across the traverses of the *P. lobata* and *A. palmata* sections are summarised in Figures 2 and 3 respectively, and the refinement summaries are given in Tables 6 and 7. The SIMS traverses across areas of the *P. lobata* sections, which were not analysed by microEXAFS, are shown in Figure 5. Transmitted light micrographs indicate the positions of fasciculi and COCs. COCs appear as dark lines or blobs, and fasciculi are composed of needle crystals which radiate out from the COCs. In the traverse of *P. lobata*, we performed the microEXAFS analyses directly along a track that had previously been produced by SIMS analyses. SIMS uses an O^- ion beam to induce sputtering, and chemical analysis is achieved by passing the resultant secondary ions into a mass spectrometer (see above). We observed that the amplitude of the resultant EXAFS was significantly reduced when compared with spectra from the other corals where microEXAFS and SIMS measurements were not directly superimposed. After refinement, the loss of amplitude is expressed as N values that are consistently less than stoichiometry. The ion track is ~30 μm wide and <5 μm deep, and therefore it is unlikely that the reduced EXAFS is a steric effect caused by shielding of the detector by the sides

Table 5. Sr/Ca determinations and refinements of microEXAFS in three coral species in relation to coral skeletal architecture. The data are refined using a fixed σ^2 refinement protocol using $\sigma_1^2 = 0.022$ Å^2, $\sigma_2^2 = 0.038$ Å^2, and $\sigma_3^2 = 0.028$ Å^2 (Finch et al., 2003a).

	Centre of calcification	Fasciculi	Fasciculi	Dissepiment
Pavona clavus				
E_f	−9.29 ± 0.33	−9.75 ± 0.36	−9.62 ± 0.37	−9.87 ± 0.39
N_1	10.52 ± 0.53	10.24 ± 0.57	10.642 ± 0.59	10.19 ± 0.61
N_2	7.81 ± 1.31	7.87 ± 1.46	8.74 ± 1.48	8.68 ± 1.52
N_3	6.95 ± 1.23	6.48 ± 1.23	6.06 ± 1.13	5.70 ± 1.17
R_1(Å)	2.595 ± 0.005	2.604 ± 0.006	2.607 ± 0.006	2.610 ± 0.006
R_2(Å)	2.973 ± 0.023	3.001 ± 0.025	3.000 ± 0.022	3.000 ± 0.024
R_3(Å)	4.019 ± 0.015	4.019 ± 0.017	4.027 ± 0.016	4.028 ± 0.017
PERCA1	99 ± 14%	106 ± 19%	118 ± 21%	118 ± 24%
R	29.78%	32.87%	32.24%	34.81%
Sr/Ca mmol mol^{-1}	10.202	9.196	9.040	9.067, 9.070
Montastrea annularis				
E_f	−8.60 ± 0.37	−9.32 ± 0.35	−9.66 ± 0.31	
N_1	10.72 ± 0.63	11.66 ± 0.63	11.92 ± 0.56	
N_2	5.29 ± 1.36	6.45 ± 1.45	8.15 ± 1.27	
N_3	5.97 ± 1.11	8.57 ± 1.36	8.08 ± 1.22	
R_1(Å)	2.572 ± 0.007	2.592 ± 0.006	2.598 ± 0.005	
R_2(Å)	2.939 ± 0.039	3.011 ± 0.029	3.007 ± 0.021	
R_3(Å)	4.014 ± 0.016	4.019 ± 0.014	4.023 ± 0.013	
PERCA1	127 ± 24%	101 ± 20%	100 ± 15%	
R	33.08%	29.93%	29.42%	
Sr/Ca mmol mol^{-1}	9.428	9.164	9.026	
Porites lobata				
E_f	−8.53 ± 0.39	−9.37 ± 0.47	−8.80 ± 0.42	
N_1	10.25 ± 0.56	9.65 ± 0.63	10.35 ± 0.60	
N_2	4.79 ± 1.42	5.36 ± 1.68	5.83 ± 1.53	
N_3	7.73 ± 1.30	7.71 ± 1.45	5.94 ± 1.16	
R_1(Å)	2.581 ± 0.006	2.608 ± 0.006	2.601 ± 0.006	
R_2(Å)	2.981 ± 0.038	3.028 ± 0.034	3.011 ± 0.031	
R_3(Å)	4.010 ± 0.014	4.033 ± 0.015	4.023 ± 0.017	
PERCA1	99 ± 17%	99 ± 14%	117 ± 23%	
R	30.89%	35.06%	33.74%	
Sr/Ca mmol mol^{-1}	9.205	8.924	8.990	

of the track from the secondary X-rays generated at the bottom. An alternative explanation may be that SIMS has caused significant amorphization of the aragonite. The interaction between an ion beam and a solid can be modelled by standard packages such as SRIM. Calculations of the implantation depth for O^- ions in aragonite at the conditions used for SIMS suggest that mean implantation depth of the ions would be ~30 nm, and that 95% of structural modification would occur between ~5 and 55 nm. Such modelling argues against significant, deep (μm) modification of the structural state of the aragonite during SIMS. Furthermore, SIMS was carried out several months before the microEXAFS, and it is unlikely that an ionic solid such as aragonite would remain amorphous in air over such periods. We remain unclear as to the origin of the reduced EXAFS amplitude. Whatever its cause, we subsequently performed microEXAFS *before* SIMS to maintain the quality of the microEXAFS data. All microEXAFS analyses across both COCs and fasciculi refine within error to values for single-phase aragonite. Errors in N_3, R_3, and PERCA1, values that would increase substantially if the material were dual phase, are similar to values in the standards (Table 2) and other point analyses (Tables 5 and 7).

In summary, all the refinements indicate that Sr is ideally substituted in aragonite (within the limits of detection discussed above) and there is no evidence for the presence of strontianite or intermediate states of order. Sr structural state does not vary in relation to skeletal architecture. In interpreting our data, we need to consider the relative contribution that each structure may make to an analysis. We selected areas for analysis where coral filled the depth of the section. In microEXAFS, the incident X-ray beam penetrates the entire thickness of the section, and in the case of fasciculi and dissepiments we are confident that these structures filled the depth of the section. However, COCs have diameters of up to 10 μm and do not fill the depth of the section. The interaction of the X-ray beam with the COCs and fasciculi in the thin section is summarised in Figure 6. Whether the COC is parallel or perpendicular to the plane of the section, we can expect that, providing the section is carefully aligned, the X-ray beam will encounter COC in the topmost 10 μm of the slide and fasciculi in the remaining underlying section of the slide. Although the X-ray beam penetrates the entire thickness of the section, the intensity of the secondary X-rays observed by the detector is greater from the top of the section. Assuming a thin section thickness of 30 μm, we estimate that the percentage of secondary X-rays recorded by the detector from depths of 0–10 μm and 10–30 μm within the section (corresponding to actual analytical depths of 0–14 μm and 14–42 μm) will be 87% and 58% respectively (Criss, 1977). For simplicity we assume a homogeneous distribution of Sr and calculate that, of the total Sr counts collected, ~43%

Table 6. Refinements along the microEXAFS traverse in the *Porites lobata* thin section.[a]

	1	2	3	4	5	6	7	8
E_f	−8.64 ± 0.56	−8.61 ± 0.50	−8.74 ± 0.52	−8.52 ± 0.42	−8.37 ± 0.35	−8.83 ± 0.31	−8.99 ± 0.33	−9.24 ± 0.29
N_1	5.64 ± 0.45	6.16 ± 0.47	7.62 ± 0.53	8.80 ± 0.51	9.61 ± 0.47	11.63 ± 0.48	10.59 ± 0.47	10.89 ± 0.43
N_2	3.84 ± 1.15	3.94 ± 1.21	4.54 ± 1.39	3.87 ± 1.36	3.81 ± 1.21	5.61 ± 1.26	4.51 ± 1.21	5.02 ± 1.13
N_3	4.54 ± 1.05	4.91 ± 1.09	6.00 ± 1.17	7.86 ± 1.15	7.82 ± 1.09	9.42 ± 1.14	8.38 ± 1.10	8.67 ± 1.02
R_1(Å)	2.567 ± 0.008	2.563 ± 0.007	2.571 ± 0.007	2.563 ± 0.006	2.563 ± 0.005	2.570 ± 0.004	2.569 ± 0.004	2.570 ± 0.004
R_2(Å)	2.980 ± 0.033	2.977 ± 0.035	3.001 ± 0.032	2.990 ± 0.037	2.982 ± 0.037	2.982 ± 0.027	2.977 ± 0.032	2.993 ± 0.028
R_3(Å)	4.012 ± 0.017	4.010 ± 0.017	4.015 ± 0.015	4.007 ± 0.011	4.002 ± 0.012	4.007 ± 0.010	4.006 ± 0.011	4.009 ± 0.010
PERCA1	100 ± 16%	103 ± 17%	106 ± 17%	104 ± 12%	100 ± 14%	100 ± 12%	100 ± 13%	100 ± 12%
R	36.77%	38.83%	33.16%	29.78%	27.85%	23.74%	25.87%	22.51%
	9	10	11	12	13	14	15	16
E_f	−8.77 ± 0.26	−8.85 ± 0.66	−8.57 ± 0.49	−9.18 ± 0.66	−8.42 ± 0.60	−8.29 ± 0.74	−8.68 ± 0.57	−8.65 ± 0.58
N_1	12.52 ± 0.44	4.98 ± 0.44	5.18 ± 0.39	5.94 ± 0.56	5.98 ± 0.49	6.01 ± 0.60	6.38 ± 0.51	7.19 ± 0.58
N_2	6.23 ± 1.16	2.96 ± 1.16	3.16 ± 1.02	3.60 ± 1.45	3.62 ± 1.34	4.07 ± 1.55	4.57 ± 1.31	5.02 ± 1.51
N_3	8.03 ± 1.06	4.42 ± 1.06	4.36 ± 0.94	5.56 ± 1.38	5.30 ± 1.20	5.08 ± 1.39	5.33 ± 1.15	6.10 ± 1.35
R_1(Å)	2.550 ± 0.003	2.565 ± 0.008	2.564 ± 0.008	2.589 ± 0.009	2.573 ± 0.008	2.578 ± 0.010	2.578 ± 0.007	2.576 ± 0.008
R_2(Å)	2.977 ± 0.025	3.003 ± 0.042	2.985 ± 0.039	3.022 ± 0.045	2.991 ± 0.036	2.995 ± 0.039	2.999 ± 0.030	3.006 ± 0.032
R_3(Å)	4.024 ± 0.011	4.007 ± 0.018	4.011 ± 0.016	4.027 ± 0.019	4.022 ± 0.017	4.015 ± 0.020	4.025 ± 0.016	4.021 ± 0.017
PERCA1	100 ± 13%	98 ± 23%	100 ± 15%	98 ± 14%	100 ± 13%	101 ± 18%	100 ± 15%	100 ± 15%
R	21.51%	37.75%	36.02%	40.93%	37.32%	41.43%	36.89%	38.70%

[a]This transverse had been previously analysed by SIMS. The sudden increase in the R-factor between points 9 and 10 is due to a reduction of the intensity of the primary beam leading to noisier data. Centres of calcification were encountered near to points 2–3 and 13. The σ^2 values used were $\sigma_1^2 = 0.022$ Å^2, $\sigma_2^2 = 0.038$ Å^2, and $\sigma_3^2 = 0.028$ Å^2 (Finch et al., 2003a).

will come from the COC and 57% from the fasciculi. However, as Sr/Ca ratios are higher in COCs, the contribution of Sr from the COC is likely to be higher than this by several %. Therefore the COC constitutes ~50% of the Sr counts with the surrounding fasciculi accounting for the remainder.

We have concluded that the limit of detection of strontianite in microEXAFS is similar to that estimated for bulk EXAFS, i.e., 5% (Finch et al., 2003a). However, if the COC only contributes, e.g., 50% of the Sr counts, and single-phase aragonite of the fasciculi contributes the remainder, the effective limit of detection of strontianite in the COC is doubled. Nevertheless, we can conclude that Sr in the COCs, as in the fasciculi, is predominantly present substituted ideally into aragonite.

Although we are confident that strontianite is not a major component of the Sr in coral aragonite, we have considered the possibility that Sr may be hosted in other crystalline phases such as celestine ($SrSO_4$) or other carbonates such as calcite ($CaCO_3$). Metal sites in calcite are smaller than those in aragonite and hence the larger Sr ion is unlikely to be preferentially hosted in that mineral. Celestine has larger interatomic distances than aragonite and, as with strontianite, significant amounts of this phase would be expressed as deviations in third shell parameters. Importantly, R-factors for modelling as single-phase aragonite are very good (~32%), often better than the refinements of standard powders, and this argues against substantial amounts of other crystalline phases.

3.2. Variations in Sr/Ca Across Skeletal Structures

The SIMS data indicate that most COCs contain more Sr than the adjacent fasciculi (Figs. 3, 4, 5a, and 5c). However this was not observed in all analyses e.g., in Figure 5b no Sr peak is associated with the COC, although a scanning electron micrograph confirms that the COC is present at the sample surface. We observe large variations (e.g., from 8.8 to 11.1 mmol mol^{-1}, see Fig. 5) in the Sr/Ca composition of COCs in the *Porites lobata* coral. The annual range of average daily temperatures at the sample site of this coral is usually ~5°C (Allison and Finch, 2004). The sensitivity of coralline Sr/Ca to temperature change is typically ~0.06–0.08 mmol mol^{-1} °C^{-1}, although a lower sensitivity has been reported for COCs

Table 7. Refinements along the microEXAFS traverse in the *Acropora palmata* section.[a]

	1	2	3	4	5	6	7	8
E_f	−14.48 ± 0.44	−8.93 ± 0.52	−12.10 ± 0.37	−11.83 ± 0.36	−11.10 ± 0.33	−10.73 ± 0.39	−10.49 ± 0.35	−10.45 ± 0.34
N_1	9.13 ± 0.57	7.70 ± 0.53	9.36 ± 0.46	9.18 ± 0.44	8.99 ± 0.38	8.77 ± 0.45	8.67 ± 0.40	8.30 ± 0.39
N_2	5.61 ± 1.48	5.27 ± 1.40	3.54 ± 1.25	5.47 ± 1.17	4.78 ± 1.01	5.18 ± 1.20	5.35 ± 1.07	4.88 ± 1.04
N_3	6.70 ± 1.29	6.58 ± 1.24	8.02 ± 1.03	7.31 ± 1.02	7.36 ± 0.87	7.48 ± 1.04	7.34 ± 0.93	7.40 ± 0.90
R_1(Å)	2.595 ± 0.006	2.573 ± 0.007	2.568 ± 0.005	2.586 ± 0.005	2.578 ± 0.004	2.580 ± 0.005	2.581 ± 0.004	2.574 ± 0.005
R_2(Å)	3.016 ± 0.031	3.006 ± 0.029	3.023 ± 0.043	3.022 ± 0.025	3.021 ± 0.025	3.018 ± 0.027	3.023 ± 0.023	3.026 ± 0.024
R_3(Å)	4.027 ± 0.016	4.018 ± 0.015	4.001 ± 0.011	4.015 ± 0.011	4.008 ± 0.009	4.016 ± 0.011	4.012 ± 0.010	4.011 ± 0.010
PERCA1	101 ± 16%	99 ± 19%	100 ± 14%	100 ± 14%	100 ± 12%	100 ± 14%	100 ± 13%	100 ± 12%
R	34.12%	33.36%	27.58%	26.56%	25.96%	27.18%	26.14%	26.92%

[a] A centre of calcification was encountered at point 4. The σ^2values used were $\sigma_1^2 = 0.022$ Å^2, $\sigma_2^2 = 0.038$ Å^2, and $\sigma_3^2 = 0.028$ Å^2 (Finch et al., 2003a).

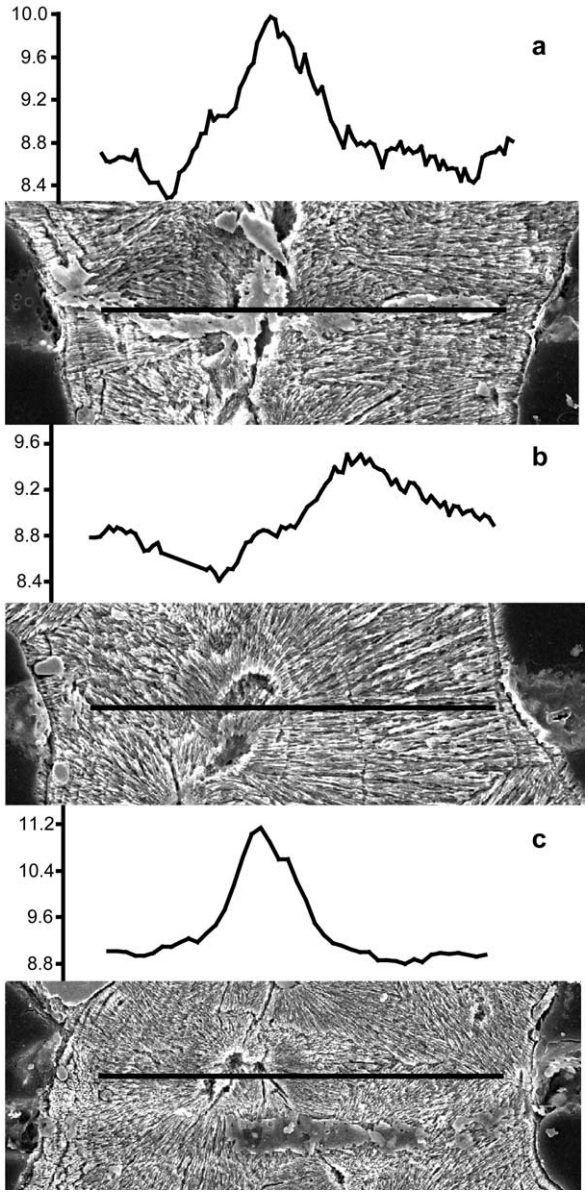

Fig. 5. Sr/Ca ratios (mmol mol^{-1}) along three transects across thin sections cut from low-density (a and b) and high-density (c) skeletal bands of the *P. lobata* coral. These sample areas were not analysed by microEXAFS. The location of each transect is shown by the black line on each scanning electron micrograph. Micrographs were produced after etching the slides for 20 s in 2% ethanoic acid, and they indicate the positions of fasciculi and COCs. The sections were gold coated after analysis but before etching, and a residue of the gold coat can be seen along the transect in (a). Each transect length = 100 μm.

(Cohen et al., 2001). Clearly Sr/Ca variations between COCs in the *P. lobata* coral studied here are not solely temperature dependent. These observations are in agreement with Allison and Finch (2004) who also reported large variations in the Sr/Ca composition of the COCs of *Porites lobata* corals which were not temperature related.

This study demonstrates that variations in Sr composition between fasciculi and COCs are not accompanied by changes in Sr structural state. If Sr compositional heterogeneity is not

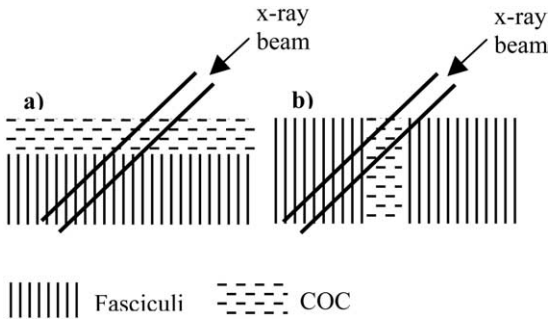

Fig. 6. Schematic diagram indicating the interaction of the X-ray beam with COCs which are (a) parallel or (b) perpendicular to the plane of the section. Assuming a section depth of 30 μm, the beam encounters a depth of ~10 μm of COC at the top of the section and a depth of ~20 μm of fasciculi at the bottom of the section.

related to partitioning of a single fluid with material of different structural states, then the causes must be sought elsewhere. The heterogeneity may result from biological or kinetic effects, or a combination of both. Kinetic effects reflect complex disequilibrium processes during crystal precipitation. Among kinetic explanations for the heterogeneity, the role of variations in crystal habit (shape) has been highlighted. The habits of the aragonite crystals are markedly different between the fasciculi (acicular crystals) and the COCs (equant crystals). The selective partitioning of trace elements onto different crystal faces, leading to compositional variations as a function of crystal habit, is well established in many mineral systems. For example, Sr has different distribution coefficients for different faces in calcite at crystal growth rates (~10–40 μm day^{-1}) which are similar to those of corals (Paquette and Reeder, 1995). Sr is incorporated onto the {1014} form faces in calcite at spiral dislocations on the crystal face, and therefore dislocation density has an important control over partitioning (Paquette and Reeder, 1995). Aragonite, like calcite, is a dominantly ionic solid, and similar mechanisms may operate. Furthermore, differences in element partitioning between crystal faces in aragonite may be more marked, because aragonite has lower symmetry than calcite and therefore a greater number of crystallographically distinct crystal faces. Sr heterogeneity in inorganic aragonite speleothems is believed to result from such differential partitioning (Finch et al., 2003b).

Biological effects result from variations in the composition of the calcifying fluid which are biologically mediated. So possible explanations for Sr heterogeneity in coral skeletons focus on potential variations in Sr and Ca transport processes to the calcification site. Coral calcification processes are not fully understood and are reviewed by Gattuso et al. (1999) and by Cohen and McConnaughey (2003). In summary, Ca is transported from seawater to the calcification site by transcellular transport (which is energy dependent) and by paracellular diffusion (i.e., through cell junctions, which is energy independent). Interpretations of Sr transport mechanisms conflict, with different authors concluding that transport is transcellular (e.g., Ferrier-Pages et al., 2002) or paracellular (Ip and Krishnaveni, 1991; Ip and Lim, 1991). Although the Sr transport mechanism may be unclear, Sr incorporation in the skeleton is inversely related to calcification rate (Ferrier-Pages et al., 2002), indicating that Sr and Ca transport are decoupled. Sr and Ca are either

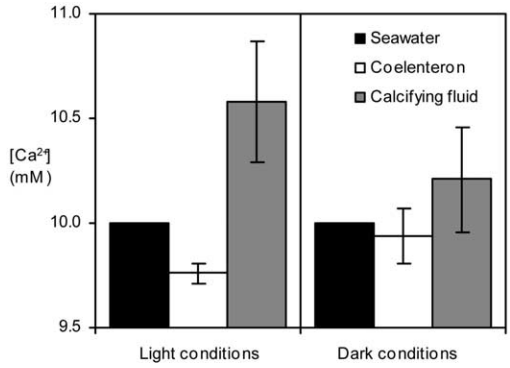

Fig. 7. Ca^{2+} concentrations in the calcifying fluid, seawater and fluid in the coelenteron, under light and dark conditions in a *Galaxea fascicularis* coral (after Al-Horani et al., 2003).

transported through different pathways or they have different transport rates through the same pathways. For example, active Ca transport across the basal coral tissues, which overlie the calcification site, occurs via Ca^{2+}-ATPase, an enzyme with a higher affinity for Ca^{2+} than for Sr^{2+} (Yu and Inesi, 1995).

Calcification rates in hermatypic corals are not constant. Dark calcification rates are typically 3–4 times lower than rates in the light (Gattuso et al., 1999; Houlbreque et al., 2003), and a reduction in calcification rate explains the higher Sr/Ca ratios usually observed in the COCs deposited at night compared with the fasciculi deposited during the day. The low Sr/Ca ratios occasionally observed in the COCs (Fig. 5b) may be deposited during periods of relatively rapid night calcification, e.g., shortly after sunset (Vago et al., 1997). Night calcification rates are affected by zooplankton availability (Houlbreque et al., 2003) and can also vary during the nightly cycle (Vago et al., 1997), offering an explanation for the non–temperature-dependent Sr/Ca variations observed across COCs in this study.

Our observation of large Sr/Ca variations between COCs in the *Porites lobata* coral is in contrast with Cohen et al. (2001) who observed only minor variations in the Sr/Ca ratios of COCs across an annual coral band and concluded that analysis of COCs offered reliable estimates of water temperatures. Cohen and McConnaughey (2003) reason that COCs may indicate seawater temperature because Ca^{2+}-ATPase does not operate at night and Sr and Ca are both transported to the calcification site by passive diffusion. As a consequence, the Sr/Ca ratio of the calcifying fluid is similar to that of seawater and the Sr/Ca composition of the deposited skeleton is predominantly affected by seawater temperature. However, evidence that Ca^{2+}-ATPase is not operative at night is inconclusive. Al-Horani et al. (2003) measured changes in the calcium concentration ($[Ca^{2+}]$) of the calcifying fluid of a *Galaxea fascicularis* coral under light and dark conditions. Under light conditions they observed a significant increase in the $[Ca^{2+}]$ of the calcifying fluid compared to ambient seawater and to fluid in the coelenteron (the body cavity which forms the fluid reservoir on the other side of the basal coral tissue to the calcification site). They observed no significant differences in the $[Ca^{2+}]$ of the three fluids under dark conditions (Fig. 7). The increase during light conditions was inhibited by ruthenium red, a specific inhibitor of Ca^{2+}-ATPase, and they concluded that Ca^{2+}-ATPase pumped Ca^{2+} to the calcification site under light conditions. However, the sensitivity of Ca microsensors may not be sufficient to record changes in $[Ca^{2+}]$ when calcification rates are low (Marshall and Clode, 2003). Dark calcification rates are typically 3–4 times lower than rates in the light (e.g., Houlbreque et al., 2003), and it is probable that the $[Ca^{2+}]$ of the calcifying fluid is lower in the dark than in the light. It is therefore unlikely that a significant increase in the $[Ca^{2+}]$ of the calcifying fluid would have been detected, given the typical reproducibility of measurement reported in the study (Fig. 7). Furthermore, Marshall (1996) reported that ruthenium red depressed both light and dark calcification by similar amounts (~40%) in a zooxanthellate coral. This implies that Ca^{2+}-ATPase does operate at night. Variations in the activity of this enzyme may provide an explanation for non–temperature-dependent Sr/Ca heterogeneity across COCs. Our data indicate that the Sr composition of COCs is affected by biological or kinetic processes, as well as temperature.

4. CONCLUSIONS

We have found no evidence for any coordination in Sr other than single-phase aragonite in any of the samples analysed. This observation is encouraging for researchers attempting to reconstruct past climates from the Sr/Ca of coral skeletons. The free energy of formation of a solid solution is different from that of a two-phase mixture, and the inclusion of Sr in more than one structural state would have complicated the relationship between Sr incorporation and SST. Although Sr/Ca composition varies substantially, both within and between different skeletal features, this is not accompanied by a change in Sr structural state. The source of this heterogeneity remains unresolved but may reflect variations in biological processes (e.g., variations in Ca transport enzyme activities affecting the composition of the calcifying fluid from which the skeleton is precipitated) or kinetic processes (e.g., variations in Sr partitioning between crystal faces affecting the Sr concentration of different crystal shapes of the skeleton). Further work is required to resolve the source of the Sr heterogeneity and to explore how kinetic and biological processes vary between coral species and coral reef sites.

The Sr/Ca composition of skeletal COCs is significantly different from that of adjacent fasciculi (Cohen et al., 2001; Allison and Finch, 2004) and Cohen et al. (2001) suggest that biological and kinetic effects may be minimised in the COCs. In this study, we observe Sr heterogeneity within both COCs and fasciculi and we conclude that there are similar challenges in reconstructing SST records from both of these skeletal structures.

Acknowledgments—This work was supported by UK Natural Environment Research Council grants NER/A/S/2001/00642 and NER/M/2000/01374. NERC Scientific Services provided access to the ion microprobe, and we are indebted to Richard Hinton (University of Edinburgh) for his assistance with the analyses. GeoSoilEnviroCARS is supported by the U.S. National Science Foundation (EAR-9906456) and U.S. Department of Energy (DE-FG02-94ER14466). Use of the Advanced Photon Source was supported by the U.S. Department of Energy under Contract No. W-31-109-Eng-38. We also wish to thank Nick Pingitore and Glen Shen for supplying samples of some of the corals analysed here. We

thank three anonymous reviewers and David Lea (Associate Editor) for insightful comments which improved this manuscript.

Associate editor: D. Lea

REFERENCES

Al-Horani F. A., Al-Moghrabi S. M., and de Beer D. (2003) The mechanism of calcification and its relation to photosynthesis and respiration in the scleractinian coral *Galaxea fascicularis*, *Mar. Biol.* **142,** 419–426.

Allison N. (1996) Geochemical anomalies in coral skeletons and their possible implications for palaeoenvironmental analysis. *Marine Chemistry* **55,** 367–379.

Allison N. and Finch A. A. (2004) High resolution Sr/Ca records in modern *Porites lobata* corals: Effects of skeletal extension rate and architecture. *Geochem. Geophys. Geosys.* **5,** doi:10.1029/2004GC000696.

Cohen A. L., Lane G. D., Hart S. R., and Lobel P. S. (2001) Kinetic control of skeletal Sr/Ca in a symbiotic coral: Implications for the palaeotemperature proxy. *Paleoceanography* **16,** 20–26.

Cohen A. L. and McConnaughey T. A. (2003) Geochemical perspectives on coral mineralization. *Rev. Mineral Geochem.* **54,** 151–187.

Criss J. W. (1977) NRLXRF–Cosmic program #DOD-00065, U.S. Naval Research Laboratory.

de Villiers S., Shen G. T., and Nelson B. K. (1994) The Sr/Ca-temperature relationship in coralline aragonite: Influence of variability in (Sr/Ca)seawater and skeletal growth parameters. *Geochim. Cosmochim. Acta* **58,** 197–208.

Eng P. J., Newville M., Rivers M. L., and Sutton S. R. (1998) Dynamically figured Kirkpatrick-Baez x-ray micro-focusing optics. In *X-ray Microfocusing: Applications and Technique* (ed. I. McNulty). *SPIE Proceedings* **3449,** 145–156.

Ferrier-Pages C., Boisson F., Allemand D., and Tambutte E. (2002) Kinetics of strontium uptake in the scleractinian coral *Styophora pistillata*. *Mar. Ecol. Progr. Ser.* **245,** 93–100.

Finch A. A. and Allison N. (2003) Strontium in coral aragonite: 2. Sr co-ordination and the long-term stability of coral environmental records. *Geochim. Cosmochim. Acta* **67,** 4519–4527.

Finch A. A., Allison N., Sutton S. R., and Newville M. (2003a) Strontium in coral aragonite: 1. Characterisation of Sr co-ordination by EXAFS. *Geochim. Cosmochim. Acta* **67,** 1189–1194.

Finch A. A., Shaw P. A., Holmgren K., and Lee-Thorp J. (2003b) Corroborated rainfall records from aragonitic stalagmites. *Earth Planet. Sci.* Lett. **215,** 265–273.

Gagan M. K., Ayliffe L. K., Hopley D., Cali J. A., Mortimer G. E., Chapell J., McCulloch M. T., and Head M. J. (1998) Temperature and surface ocean water balance of the mid-Holocene tropical western Pacific. *Science* **279,** 1014–1018.

Gattuso J. P., Allemand D., and Frankignoulle M. (1999) Photosynthesis and calcification at cellular, organismal and community levels in coral reefs: A review on interactions and control by carbonate chemistry. *Am. Zool.* **39,** 160–183.

Gladfelter E. H. (1983) Skeletal development in *Acropora cervicornis.* II Diel patterns of calcium carbonate accretion. *Coral Reefs* **2,** 91–100.

Greegor R. B., Pingitore N. E. Jr., and Lytle F. W. (1997) Strontianite in coral skeletal aragonite. *Science* **275,** 1452–1454.

Houlbreque F., Tambutte E., and Ferrier-Pages C. (2003) Effect of zooplankton availability on the rates of photosynthesis and tissue and skeletal growth in the scleractinian coral *Stylophora pistillata*. *J. Exp. Mar. Biol.* **296,** 145–166.

Ip Y. K. and Krishnaveni P. (1991) Incorporation of strontium ($^{90}Sr^{2+}$) into the skeleton of the hermatypic coral *Galaxea fascicularis*. *J. Exp. Zool.* **258,** 273–276.

Ip Y. K. and Lim A. L. L. (1991) Are calcium and strontium transported by the same mechanism in the hermatypic coral *Galaxea fascicularis*? *J. Exp. Biol.* **159,** 507–513.

Jarosch D. and Heger G. (1988) Neutron diffraction investigation of strontianite, $SrCO_3$. *Bull. Minéral.* **111,** 139–142.

Marshall A. T. (1996) Calcification in hermatypic and ahermatypic corals. *Science* **271,** 637–639.

Marshall A. T. and Clode P. L. (2003) Light-regulated Ca^{2+} uptake and O^{-2} secretion at the surface of a scleractinian coral *Galaxea fascicularis*. *Comp. Biochem. Phys. A* **136,** 417–426.

Paquette J. and Reeder R. J. (1995) Relationship between surface-structure, growth-mechanism and trace-element incorporation in calcite. *Geochim. Cosmochim. Acta* **59,** 735–749.

Schneider R. C. and Smith S. V. (1982) Skeletal Sr content and density in *Porites spp* in relation to environmental factors. *Mar. Biol.* **66,** 121–131.

Sutton S. R., Bertsch P. M., Newville M., Rivers M., Lanzirotti A., and Eng P. (2002) Microfluorescence and microtomography analyses of heterogeneous Earth and environmental materials. *Reviews in Mineralogy and Geochemistry* **49,** 429–483.

Vago R., Gill E., and Collingwood J. C. (1997) Laser measurements of coral growth. *Nature* **386,** 30–31.

Yu X. and Inesi G. (1995) Variable stoichiometric efficiency of Ca^{2+} and Sr^{2+} transport by the sarcoplasmic-reticulum Atpase. *J. Biol. Chem.* **270,** 4361–4367.

ELECTRONIC ANNEX

Supplementary data associated with this article can be found, in the online version, at doi:10.1016/j.gca.2005.01.026.